A&A 470, 249–257 (2007)
DOI: 10.1051/0004-6361:20066779

Astronomy & Astrophysics

XMM-Newton observations of HESS J1813−178 reveal a composite Supernova remnant

S. Funk[1,2], J. A. Hinton[3], Y. Moriguchi[1,4], F. A. Aharonian[5,1], Y. Fukui[4], W. Hofmann[1], D. Horns[6], G. Pühlhofer[7], O. Reimer[8], G. Rowell[9], R. Terrier[10], J. Vink[11], and S. J. Wagner[7]

[1] Max-Planck-Institut für Kernphysik, PO Box 103980, 69029 Heidelberg, Germany
[2] Kavli Institute for Astroparticle Physics and Cosmology, SLAC, PO Box 0029, 94025, USA
e-mail: Stefan.Funk@slac.stanford.edu
[3] School of Physics & Astronomy, University of Leeds, Leeds LS2 9JT, UK
[4] Department of Astrophysics, Nagoya University, Chikusa-ku, Nagoya 464-8602, Japan
[5] Dublin Institute for Advanced Studies, 5 Merrion Square, Dublin 2, Ireland
[6] Institut für Astronomie und Astrophysik, Universität Tübingen, Sand 1, 72076 Tübingen, Germany
[7] Landessternwarte, Universität Heidelberg, Königstuhl, 69117 Heidelberg, Germany
[8] Stanford University, HEPL & KIPAC, Stanford, CA 94305-4085, USA
[9] School of Chemistry & Physics, University of Adelaide, Adelaide 5005, Australia
[10] APC, 11 Place Marcelin Berthelot, 75231 Paris Cedex 05, France
[11] Astronomical Institute, University Utrecht, PO Box 80000, 3508TA Utrecht, The Netherlands

Received 20 November 2006 / Accepted 2 April 2007

ABSTRACT

Aims. We present X-ray and ^{12}CO($J = 1-0$) observations of the very-high-energy (VHE) γ-ray source HESS J1813−178 with the aim of understanding the origin of the γ-ray emission.
Methods. High-angular resolution X-ray studies of the VHE γ-ray emission region are performed using 18.6 ks of *XMM-Newton* data, taken on HESS J1813−178 in October 2005. Using this data set we are able to undertake spectral and morphological studies of the X-ray emission from this object with greater precision than previous studies. NANTEN ^{12}CO($J = 1-0$) data are used to search for correlations of the γ-ray emission with molecular clouds which could act as target material for γ-ray production in a hadronic scenario.
Results. The NANTEN ^{12}CO($J = 1-0$) observations show a giant molecular cloud of mass 2.5×10^5 $M_\odot$ at a distance of 4 kpc in the vicinity of HESS J1813−178. Even though there is no direct positional coincidence, this giant cloud may have influenced the evolution of the γ-ray source and its surroundings. The X-ray data show a highly absorbed ($n_{\rm H} \sim 1. \times 10^{23}$ cm^{-2}) non-thermal X-ray emitting object coincident with the previously known ASCA source AX J1813−178 exhibiting a compact core and an extended tail towards the north-east, located in the centre of the radio shell-type Supernova remnant (SNR) G12.82–0.02. This central object shows morphological and spectral resemblance to a Pulsar Wind Nebula (PWN) and we therefore consider that this object is very likely to be a *composite SNR*. We discuss the scenario in which the γ-rays originate in the shell of the SNR, and that in which they originate in the central object, in terms of a time-dependent one-zone leptonic model. We demonstrate, that in order to connect the core X-ray emission to the VHE γ-ray emission electrons have to be accelerated to energies of at least 1 PeV.

Key words. ISM: supernova remnants – ISM: individual objects: HESS J1813−178 – ISM: individual objects: G12.82–0.02 – ISM: individual objects: AX J1813−178 – gamma rays: observations

1. Introduction

During a survey of the Galactic plane in very high-energy (VHE) γ-rays using the atmospheric Cherenkov telescope system HESS more than a dozen new >100 GeV γ-ray sources were found (Aharonian et al. 2005a, 2006a). Even though some of the new γ-ray sources can be identified with counterparts at other wavebands, for example the *microquasar* LS 5039 (Aharonian et al. 2005b, 2006b), most of them lack a compelling positional counterpart (Funk 2007). A firm counterpart identification for a γ-source at other wavebands requires not only a spatial association, but also a viable γ-ray emission mechanism and a consistent multi-frequency picture. X-ray observations with instruments such as *XMM-Newton* and *Chandra* combine high-angular-resolution and high-sensitivity observations with the possibility to trace relativistic electrons via their synchrotron emission. These instruments are thus ideally suited to the identification of VHE γ-ray objects. This article reports on multi-frequency observations of HESS J1813−178 with the *XMM-Newton* X-ray satellite. Dense molecular regions that could act as target material for hadronic interactions have been studied using the NANTEN CO-telescope to test for an origin of the γ-ray emission in the decay of neutral pions produced in proton-proton collisions.

HESS J1813−178 was in fact the first source discovered during the HESS survey, and was subsequently re-observed to increase the γ-ray signal to 340 events (with a statistical significance of ∼14 standard deviations) from a total of 9.7 h of observations. Whilst many of the new sources found in the survey exhibit rather large intrinsic extensions, HESS J1813−178 has a compact nature and is only slightly extended (Gaussian width $\sigma = 2.2' \pm 0.4'$) with respect to the point-spread function (PSF) of the HESS instrument. The flux of the source

is $(14.2 \pm 1.1_{\rm stat}) \times 10^{-12}$ photons cm^{-2} s^{-1} above 200 GeV and the energy spectrum follows a power-law with photon index 2.09 ± 0.08. HESS J1813−178 is located in the Galactic plane at $18^{\rm h}13^{\rm m}38^{\rm s}$, $-17^{\rm d}50'33''$. HESS J1813−178 was subsequently also detected by the MAGIC Cherenkov telescope confirming the basic properties of the source (Albert et al. 2006).

At the time of the first publication of this source (Aharonian et al. 2005a), HESS J1813−178 was still considered as unidentified. However, subsequently to the HESS publication, the source was reported as being in compelling positional coincidence with several objects known in other energy bands (Brogan et al. 2005; Helfand et al. 2005; Ubertini et al. 2005). HESS J1813−178 coincides with the previously unpublished archival ASCA source AX J1813−178 in the 2−10 keV band (Brogan et al. 2005). This unresolved ASCA source with a rather hard photon index of 1.8 ± 0.4 and a flux of 7×10^{-12} erg cm^{-2} s^{-1} (2−10 keV) was one of the few relatively bright sources detected in the ASCA Galactic Plane survey (Sugizaki et al. 2001). AX J1813−178 exhibits a highly absorbed ($n_{\rm H} = (1.1 \pm 0.2) \times 10^{23}$ cm^{-2}) non-thermal spectrum without indications of emission lines. The value of $n_{\rm H}$ is significantly larger than the total column density through the Galaxy in this direction, suggesting that the source is embedded in a dense environment. The unresolved hard X-ray source IGR J18135–1751 detected in the INTEGRAL Galactic plane survey in the 20–100 keV energy band also lies in positional coincidence (Ubertini et al. 2005). The energy spectrum of IGR J18135–1751 is compatible with that of the ASCA source in terms of flux, but is softer, suggesting a spectral break in the X-ray spectrum around 10 keV. Recently this source has also been detected with the *Swift* X-Ray Telescope (XRT). The XRT data confirm the hard spectral index and the high column density towards the source that were found in the ASCA data (Landi et al. 2006).

The region surrounding HESS J1813−178 was also covered by observations in the 20 cm and 90 cm band by the VLA. These data show a faint non-thermal radio source (G12.82–0.02) visible at the position of HESS J1813−178 (Brogan et al. 2005; White et al. 2005). G12.82–0.02 lies in the projected vicinity (distance $\sim 15'$) of the W 33 region. This region is known to contain ultra-compact HII regions (Churchwell 1990) and contains methanol, hydroxyl, and water masers and other tracers of recent star formation. While HESS ASCA, and INTEGRAL lack the spatial resolution to resolve this object, the angular resolution of the VLA allows a shell-like radio structure of diameter $2.5'$ to be resolved. The flux at 20 cm was reported as 0.65 ± 0.1 Jy, the flux at 90 cm was given as 1.2 ± 0.08 Jy, suggesting a non-thermal radio spectrum of index $\alpha = -0.42 \pm 0.03$ ($j_\nu \propto \nu^\alpha$). The radio spectrum and morphology led Brogan et al. (2005) to the conclusion that the radio structure is a previously unknown young shell-type Supernova remnant (SNR). *Spitzer* Space Telescope data from the GLIMPSE survey at 8 μm (Benjamin et al. 2003) show no signs of dust emission in positional coincidence with G12.82–0.02 a finding that might be expected, given that Reach et al. (2006) detected only 18 out of 95 known SNRs in the GLIMPSE survey.

In the Parkes multi-beam pulsar survey (PMBS) no pulsar close to G12.82–0.02 has been found thereby limiting the 1.4 GHz flux density to a rather constraining level of <0.2 mJy (Manchester et al. 2001). Current constraints on the distance of the object have been derived from HI absorption data (Brogan et al. 2005) as well as from the strong absorption found in the X-ray data, both suggesting that AX J1813–178 is located behind W 33 at a distance larger than 4 kpc.

Assuming an association between HESS J1813−178 and the radio source G12.82–0.02, the question remains whether the thus far unresolved X-ray and γ-ray emission originate from the shell of the SNR, or rather from a Pulsar Wind Nebula (PWN) embedded within the shell. Brogan et al. (2005) concluded from the fact that the radio spectrum nearly directly extrapolates into the ASCA X-ray spectrum, that both the radio shell and the ASCA source should indeed be the same source and therefore that all the emission was connected to the radio shell.

This article reports on high-angular resolution X-ray observations performed with *XMM-Newton* with the goal of pinning down the origin of the high-energy X-ray and γ-ray emission. Another option for the γ-ray emission is the interaction of accelerated hadrons with dense molecular material. The nearest massive molecular cloud is that associated with the W 33 star forming region, located $\sim 10'$ away from HESS J1813−178. Dense gas in the W 33 region could act as target material for the VHE γ-ray generation in hadronic interactions, therefore a study of the ^{12}CO($J = 1-0$) distribution performed during the NANTEN survey of the Galactic plane (Mizuno & Fukui 2004) towards HESS J1813−178 is included.

2. *XMM-Newton* observations of the region

HESS J1813−178 was observed with *XMM-Newton* on the 14th of October 2005 for 18.6 ks. The instrument cameras (EPIC MOS1, MOS2, PN) were operated in full-frame mode with a medium filter to screen out optical and UV light. The data were processed with the *XMM-Newton* Science Analysis Software (SAS) version 7.0 as well as with the Extended Source Analysis Software package (XMM-ESAS) version 1.0 (Snowden et al. 2004). Standard data reduction and calibration procedures were applied to the data and the total data set amounts to 13.6 ks after the observations have been cleaned of flaring background caused by soft protons. Figure 1 shows the resulting combined count map of the EMOS1 and EMOS2 detectors for three different energy bands (red: 0.5 keV to 2 keV, green: 2 keV to 4.5 keV, blue: 4.5 keV to 10 keV) smoothed with a Gaussian kernel of 3 pixels width. The X-ray morphology does not resemble the shell-like emission seen in the radio. A compact X-ray source with an extended tail towards the northwest is visible at the centre of the EMOS-Cameras. This source is in positional coincidence with the previously reported ASCA source AX J1813−178. There is some contamination of soft photons in this data set. This had been seen before in the ASCA data and can be attributed to the bright, close-by ($\sim 0.7^\circ$) low mass X-ray binary GX 13+1. To investigate the influence of the soft photon contamination in the background regions for the spectral studies, three separate methods were applied to estimate the background as discussed later in the text. The results for the different methods show good agreement, enhancing the confidence that the background level in the spectral studies was estimated correctly. There is however still the possibility of soft photon contamination in the source spectrum, especially at energies below 2 keV, since the source appears strongly absorbed below this energy.

For the source position fitting the contamination was avoided by using the source detection algorithm (*emldetect*) as described in Snowden et al. (2004) for energies above 4.5 keV and for energies above 7.5 keV. Seven sources are detected in the band above 4.5 keV which are not in the part of the field of view affected by the stray light (see Table 1), whereas above 7.5 keV only a single X-ray source is detected. This source is extended and coincident with AX J1813−178 at a best-fit position $18^{\rm h}13^{\rm m}35.16^{\rm s}$,

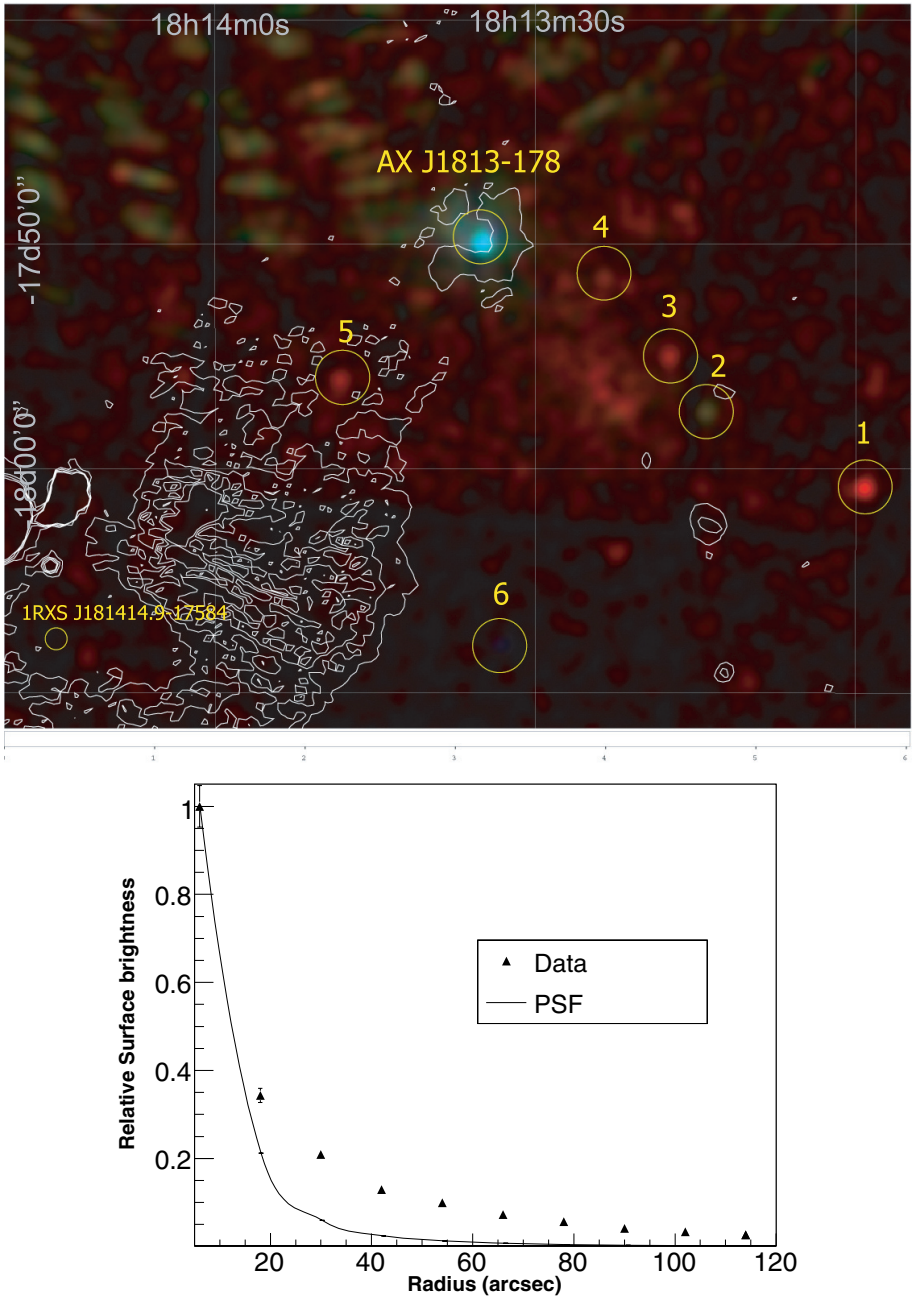

Fig. 1. *Top*: a composite false-colour image of the EMOS1 and EMOS2 count maps, slightly smoothed with a Gaussian kernel of width 3 image pixels. Different colours correspond to 0.5 keV−2 keV (red), 2 keV−4.5 keV (green), and 4.5 keV−10 keV (blue). AX J1813–178 appears as a bright, hard-spectrum source with a tail towards the north-west. The north-western edge of the field of view shows some soft stray-light contamination, caused by the low mass X-ray binary GX 13+1. Also shown are several other X-ray sources that were found with *emldetect* at energies above 4.5 keV. These are typically fainter and have a softer photon index. The white contours denote the VLA 20 cm radio emission as already reported by Brogan et al. (2005). The shell-like radio structure surrounding AX J1813–178 is clearly visible. *Bottom*: radial profile of the central source AX J1813–178 in comparison to the PSF for this data set.

$-17^{d}49'50.0''$, with a statistical error on the position of 2″. This position is at a distance of ∼1′ from the best fit position of HESS J1813−178, located well within the extension of 2.2′ of HESS J1813−178. Even though a perfect match of the best fit X-ray and γ-ray positions is not a priori expected, as seen for example in the PWN candidate HESS J1825–137 (in which the HESS position is significantly shifted from the peak of the X-ray emission, Aharonian et al. 2006c) the position of AX J1813–178 is compatible with the HESS position, given a statistical error of 21″ adding to a systematic error in the pointing accuracy of the HESS instrument of the similar size. The source position fitting tool *emldetect* also determines AX J1813–178 to be incompatible with a point-source. Using a Gaussian model the extension was determined to be 8.5 ± 0.2 image pixels, corresponding to a projected width on the sky of 21″ ± 0.5″. As apparent in the slice through the source, shown in Fig. 2, the Gaussian profile might not be the correct representation of the source profile, which seems to have a rather long tail towards the north-east. The source position determined using the *XMM-Newton* data is compatible with the position of the only X-ray source found in the *Swift* XRT data (Landi et al. 2006) at $18^{h}13^{m}34.9^{s}$, $-17^{d}49'53.2''$with an error of 3.5″. The distance of the best fit position presented here to the XRT position is 4.9″. The other sources within the field of view listed in Table 1 have no previous X-ray detection.

For the spectral analysis XSPEC (version 12.2.1) was used and three different background methods were applied to estimate the effect of stray-light contamination on the spectrum of AX J1813–178. The background was estimated a) from the south-western part of the field of view, where the stray-light contamination is apparently lower b) from a ring around the source with inner radius 100″ and outer radius 200″ and c) from blank field observations as described in Snowden et al. (2004). All three methods yield consistent results for the spectral fit. In the following the background derived from a ring around the source within the same field of view is used. Different extraction radii

Table 1. X-ray sources other than AX J1813–178 detected in the field of view surrounding HESS J1813–178 using the detection algorithm *emldetect*. The second column gives the name recommended by the *XMM-Newton* SOC and the IAU for serendipitous *XMM-Newton* source detections. Columns 3 and 4 give J2000 coordinates with a typical error on the position of 1″. Column 5 gives the number of counts in a circle of radius 30″ above 2 keV.

Id	XMMUJ	RA_{2000} (h:m:s)	Dec_{2000} (d:′:″)	Counts
1	181259.2–175527	18:12:59.23	–17:55:26.9	60
2	181314.1–175344	18:13:14.11	–17:53:44.1	238
3	181318.0–175232	18:13:17.57	–17:52:31.9	90
4	181323.7–175041	18:13:23.68	–17:50:41.2	138
5	181348.3–175301	18:13:48.35	–17:53:00.6	68
6	181333.3–175857	18:13:33.27	–17:58:56.7	157
	AX J1813–178	18:13:35.16	–17:49:50.0	2192

of size 50″, 75″, and 100″ were used to determine the spectrum of the extended emission. All EMOS1, EMOS2, and EPN data were fit simultaneously. In general the data are well described by a single power-law and the results of the spectral fitting are summarised in Table 2. Figure 3 shows the *XMM-Newton* spectrum for the medium size extraction radius of 75″. As can be seen, no prominent line emission exists and analysis shows that the shape is incompatible with a black-body radiation spectrum, confirming the non-thermal nature of the X-ray emission. The results for the different extraction radii are entirely compatible with each other in terms of column density and spectral index. The column density determined is $n_{\rm H} \sim 10^{23}$ cm^{-2}, significantly higher than the total Galactic column density in this region of the Galactic plane, 1.6×10^{22} cm^{-2} (Dickey & Lockman 1990). The photon index is determined to be ∼1.8, the flux between 2 and 10 keV for the 75″ extraction radius is $\sim 7 \times 10^{-12}$ erg cm^{-2} s^{-1}. Both these values are compatible with previous estimates from the analysis of ASCA data (photon index: 1.8 ± 0.4, $F_{2-10\ \rm keV} = 7.0 \times 10^{-12}$ erg cm^{-2} s^{-1}) by Brogan et al. (2005). It should be noted that this flux possibly contains some contamination from a non-subtracted point-source. Any such contamination is expected to cover one or two bins in the slice shown in Fig. 2 and therefore amount to at most ∼20% of the flux.

Comparing the number of counts on the shell with those in the central source a conservative upper limit of the X-ray emission on the shell of $F_{2-10\ \rm keV} = 7.0 \times 10^{-12}$ erg cm^{-2} s^{-1} can be derived. Using a Raymond-Smith model (assuming thermal equilibrium between electron and ion plasma) this upper limit can be used to determine an upper limit on the emission measure $k = n_{\rm e} n_{\rm H} V (4\pi D^2)^{-1}$ of an X-ray emitting thermal plasma under the assumption of various temperatures T (here $n_{\rm e}$ and $n_{\rm H}$ correspond to the electron and hydrogen densities in the plasma, V the volume of the plasma and D the distance). For a temperature of 1 keV, the emission measure is $k = 3.47 \times 10^{11}$ cm^{-5}, corresponding to an upper limit on the density of $n_{\rm H} = 4.1$ cm^{-3} (at a distance of 4 kpc). Assuming a density of $n_{\rm H} = 1$ cm^{-3}, the corresponding upper limit on the plasma temperature is $kT \sim 5$ keV.

The EPN data within a narrow region (5″) surrounding AX J1813–178 were searched for periodic emission from any possible X-ray pulsar. The timing resolution of the EPN detector in full-frame mode is 73.2 ms. No significant periodicity was found. Indeed no evidence for variability was detected in this data set. Future X-ray timing observations with *XMM-Newton* or *Chandra* and future Multibeam radio observations might shed further light on the existence of a pulsar at this location.

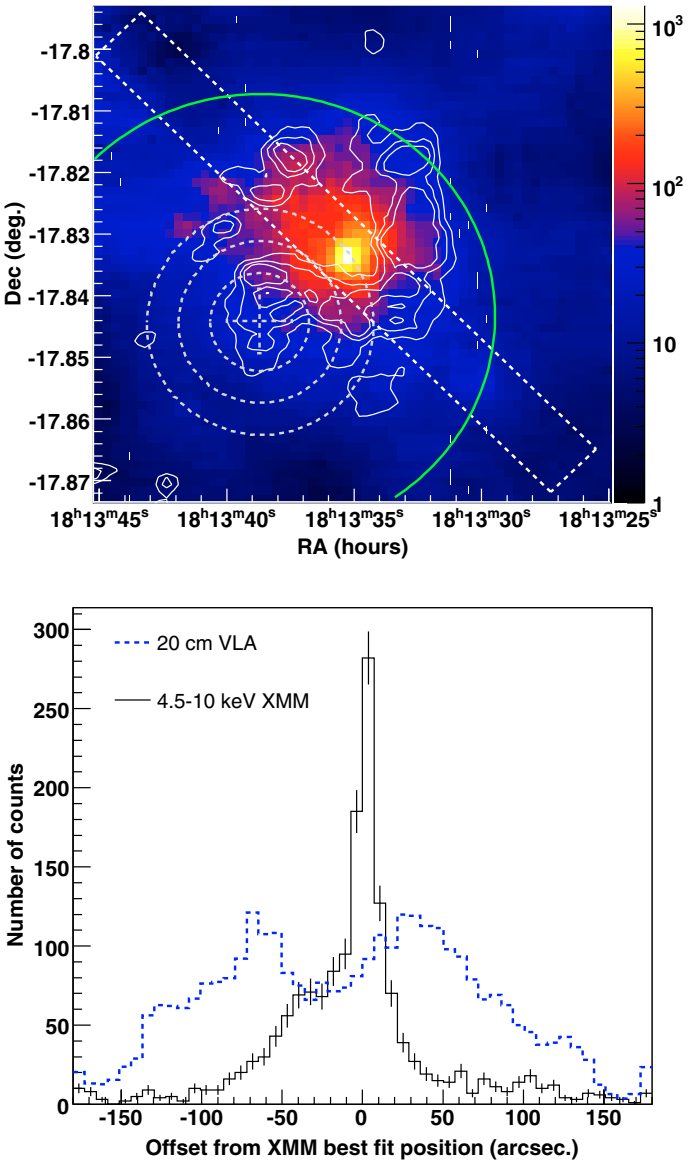

Fig. 2. Comparison of radio and X-ray data of HESS J1813−178. *Top*: *XMM-Newton* counts map above 4.5 keV of the region surrounding HESS J1813−178 (colour contours) smoothed with a Gaussian kernel of width 0.1′. The extended tail towards the north-east is visible in this figure. Overlaid is the 20 cm shell-like emission (white contours) as detected by the VLA (Brogan et al. 2005). The difference in the images between the X-ray and the radio wavebands is apparent in this figure. Also shown are the positional contours (1, 2, 3σ error) of the best fit position of HESS J1813−178 as given in Aharonian et al. (2006a) (dashed circles) and the extension (solid green), covering both the radio and X-ray emitting region completely. *Bottom*: slice through the emission in radio and X-rays as plotted on the left hand side. The box in which the slices were determined is also given in the left panel (white box). The X-ray slice shows the compact core with the slice towards the north-east, whereas the radio slice shows the shell-like structure of the emission.

3. NANTEN-observations towards HESS J1813–178

The ^{12}CO(J = 1−0) observations were performed using the 4-meter mm/sub-mm telescope, NANTEN, at Las Campanas Observatory of the Carnegie Institution of Washington, in Chile. The NANTEN ^{12}CO(J = 1−0) survey of the Galactic plane shows that the velocity of the ^{12}CO emission towards HESS J1813−178 ranges from $v_{\rm LSR}$ (*velocity local standard of*

Table 2. Spectral properties of AX J1813–178 as determined by the spectral fitting routine. EMOS1, EMOS2, and EPN data were simultaneously fit with a single absorbed power-law. The fit parameters are the column density $n_{\rm H}$, the photon index Γ, and the normalisation at 1 keV, which is expressed by the flux between 2 keV and 10 keV. Different spectral shapes such as a black-body spectrum were incompatible with the data (as an example: the χ^2/d.o.f. for a blackbody spectrum for the extraction region of size 75″ is 5700. The errors given here correspond to a 90% confidence level.

Radius	Counts			$n_{\rm H}$	Γ	$F_{2-10\ \rm keV}$	χ^2/d.o.f.
(arcsec)	EMOS1	EMOS2	EPN	10^{22} cm^{-3}		10^{-12} erg cm^{-2} s^{-1}	
50	2004	1805	3930	$12.0^{+1.0}_{-0.7}$	$1.81^{+0.16}_{-0.11}$	5.2	3177/3001
75	2957	2769	6194	$10.6^{+0.7}_{-0.7}$	$1.72^{+0.12}_{-0.12}$	6.8	3233/3001
100	3794	3592	8397	$10.6^{+0.2}_{-0.3}$	$1.88^{+0.05}_{-0.03}$	6.9	3228/3001

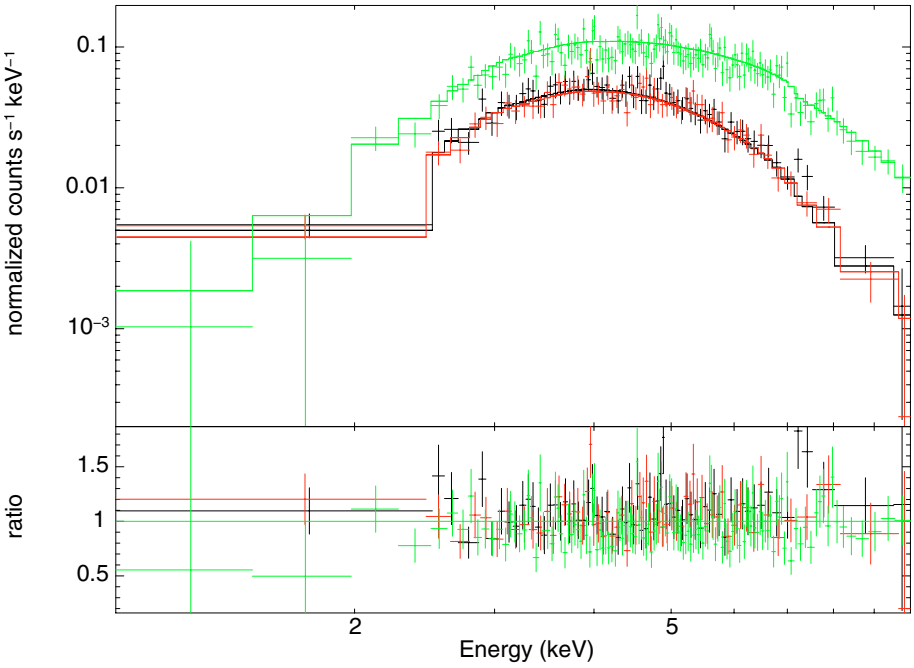

Fig. 3. *XMM-Newton* energy spectrum for all three detectors (EMOS1: black, EMOS2: red, EPN: green) for an extraction radius of 75″, rebinned to yield a minimum significance of 5σ in each bin, summing a maximum of 100 bins into a single one bin. The straight lines show the combined fit to these data (folded with the instrumental response which is different for the three detectors). The lower panel shows the residuals of the data to the fit. As can be seen, the power-law fit provides a reasonable description of the data. Also apparent is the absence of prominent line emission that lends support to the non-thermal nature of the emission.

rest, i.e. the average velocity of stars in the solar neighbourhood) ∼0 km s^{-1} to ∼60 km s^{-1}. While the CO emission at $v_{\rm LSR}$ less than 10 km s^{-1} is likely due to local clouds, the emission at velocities in excess of $v_{\rm LSR}$ ∼ 20 km s^{-1} is likely from clouds beyond 2 kpc. The best known object in the region surrounding HESS J1813−178 is W 33, a complex of HII regions, a typical example of a massive star forming region. The integrated intensity distribution at $v_{\rm LSR}$ = 30–40 km s^{-1} shows an enhancement in close projected vicinity to HESS J1813−178 as shown in Fig. 4. To convert the velocity range into a distance the model of Brand & Blitz (1993) has been used and the rather large uncertainty in kinematic distance for directions close to the Galactic centre has to be taken into account. The W 33 complex has been studied fairly extensively in the past and its distance has been estimated to be ∼4 kpc (kinematic distance derived from molecular line observations see e.g. Reifenstein et al. 1970; Goldsmith & Mao 1983; Mitchell et al. 1990). The most massive molecular cloud in the direction of HESS J1813−178 is in the velocity range 30–40 km s^{-1} as shown in Fig. 4. The size of this cloud is ∼70 pc × 40 pc in Galactic longitude and latitude (at an assumed distance of 4 kpc) and its total mass is estimated to be 2.5 × 10^5 solar masses from the ^{12}CO(J = 1–0) velocity integrated intensity, equivalent to 10^{21} cm^{-2} in molecular column density, assuming an X-factor of 2 × 10^{20} cm^{-2}/(K km s^{-1}) (Bertsch et al. 1993) (where $X = N({\rm H_2})/I({\rm CO})$, is the conversion factor between H_2 column density and integrated CO intensity). This mass is typical for a giant molecular cloud. HESS J1813−178 is clearly located outside of the dense cloud (∼20 pc away) and therefore the cloud and the VHE γ-ray emission are probably unrelated. The region surrounding HESS J1813−178 is a fairly complicated ensemble of young massive stars as indicated by several compact HII regions. Figure 5 shows *Spitzer* Space Telescope data from the GLIMPSE survey at 8 μm (Benjamin et al. 2003). As previously mentioned, no dust emission at the position of HESS J1813−178can be found (red contours denote the 1, 2, and 3σ error contours on the centroid of the VHE γ-ray emission), however, the peak in the CO-data seems to be correlated to the 8 μm data. The fact that most dust in the region that has not yet been blown away by the hot stars might suggest that these stars are still rather young. The total integrated column density determined for a beam size of 2.6′ centred on Galactic longitude 12.8, latitude 0.0 (the closest position to HESS J1813–178 in the NANTEN survey with a grid size of 4′) is ∼9 × 10^{22} cm^{-2}, somewhat higher than the value determined by Dickey & Lockman (1990) (1.6 × 10^{22} cm^{-2}), but fully consistent with the high absorption density determined from the *XMM-Newton* data. Integrating the column density only to 4 kpc, the proposed location of AX J1813–178, results in a value of ∼(0.5–1.)×10^{22} cm^{-2}. Comparing the NANTEN values presented here with the values from Dickey & Lockman (1990) the differences can be attributed to both the difference in material probed (atomic versus molecular hydrogen) and the differing angular resolution of the two surveys.

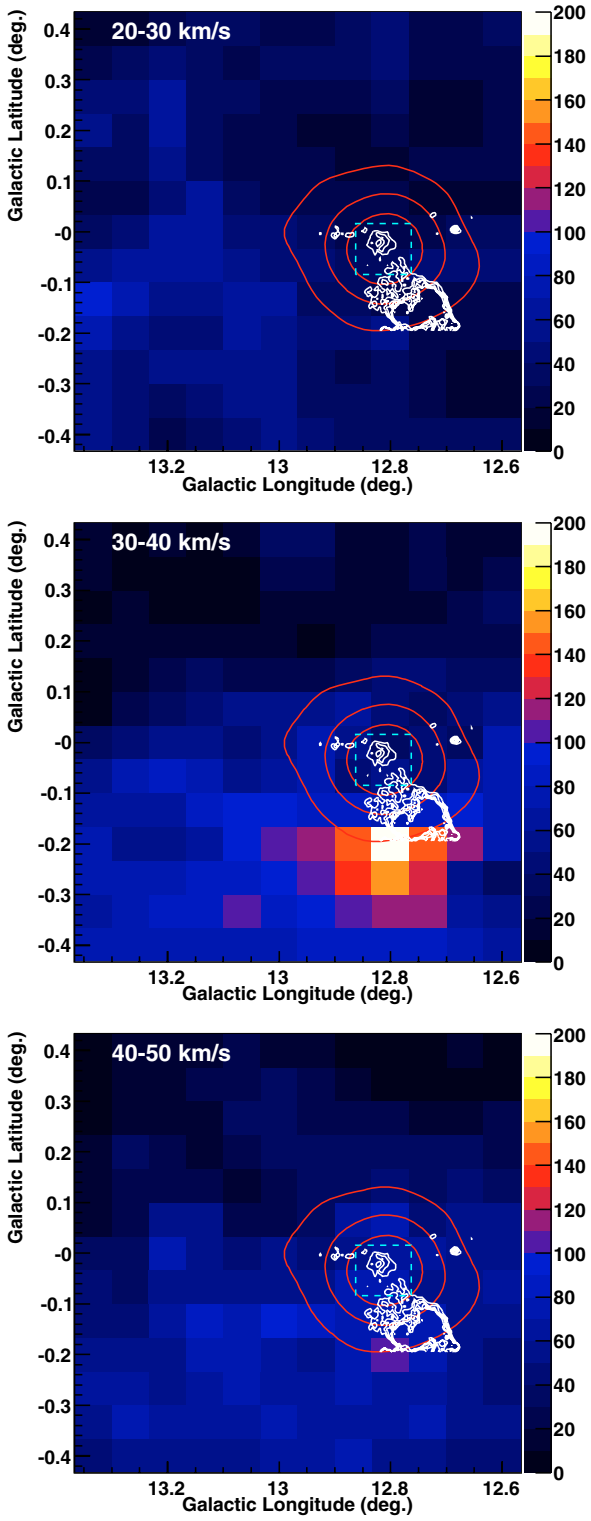

Fig. 4. NANTEN ^{12}CO(J = 1−0) data towards the region surrounding HESS J1813−178 for three different velocity ranges. Please note that this figure is in Galactic coordinates. The colour scale shows the CO emission in units of K km s^{-1}, the red contours the HESS VHE γ-ray excess emission (smoothed with a Gaussian of 0.05° width and plotted in equidistant excess contours), whereas the white contours show the 20 cm VLA contours (Brogan et al. 2005). The dashed cyan box indicates the size of the area shown in Fig. 2. The shell-type radio emission at the centre of this region is the SNR G12.82–0.02. As can be seen from this figure, the giant molecular cloud at 30−40 km s^{-1} (corresponding to ∼4 kpc) is not in coincidence with HESS J1813−178, could however be associated with the star-forming region W 33 to the south of HESS J1813−178.

4. Interpretation of the X-ray emission, connection to other wavebands

Even though the NANTEN CO-Emission is probably unrelated to HESS J1813−178, it is interesting to calculate an upper limit on the cosmic ray density in the dense molecular cloud given the non-detection of a VHE γ-ray signal. To calculate the ratio of the cosmic ray density in the cloud $\rho_{\rm CR,GMC}$ to the local cosmic ray density $\rho_{\rm CR,local}$ the following relation is used:

$$\rho_{\rm CR,GMC}/\rho_{\rm CR,local} = \frac{F_{(>1\ \rm TeV)} \times D^2}{2.85 \times 10^{-13} \times M_5 \quad (\ \rm kpc^2\ cm^{-2}/s)} \qquad (1)$$

(here $F_{(>1\ \rm TeV)}$ is the γ-ray flux above 1 TeV in units of cm^{-2} s^{-1}, D is the distance in kpc, and M_5 is the mass of the cloud in units of 10^5 solar masses) Aharonian (1991). The factor 2.85×10^{-13} kpc^2 cm^{-2}/s has been derived assuming a CR spectrum with a photon index of 2.6. Using a 2σ HESS upper limit of 0.6% of the Crab flux above 1 TeV (taken from the 10 h exposure time and the HESS sensitivity of 1% Crab flux in a 25 h observation), i.e. 1.1×10^{-13} cm^{-2} s^{-1}, a distance of D = 4 kpc, and a cloud density of M_5 = 2.5, an upper limit for $\rho_{\rm CR,GMC}$ of $\sim 3 \times \rho_{\rm CR,local}$ can be derived.

Figure 2 shows a comparison between the X-ray and radio emission in the region surrounding HESS J1813−178. As is clearly seen, the radio emission exhibits a shell-like structure whereas the X-ray emission has a compact core with extended emission towards the north-east, a typical morphology for a PWN (see Gaensler & Slane 2006, for a recent review). The apparent anti-correlation with the radio shell also suggest a confinement of the X-ray emission within the shell, especially since the tail of the X-ray source extends to the NE, where a break in the radio shell is present. The non-detection of a pulsar in reasonably deep radio observations may be due to beaming effects. In the X-ray data presented here the thermal emission from the possible neutron star might be buried underneath the strong non-thermal emission and additionally strongly absorbed by the high column density which strongly affects the detection of X-rays below ∼1.5 keV. However, to finally confirm this scenario, the pulsar within this nebula would need to be found, either in deep radio or X-ray observations. Alternative strong evidence that AX J1813–178 is a PWN would be the detection of spectral softening away from the core, a signature of electron cooling which is observed in many PWN, see for example G21.5–0.9 (Slane et al. 2000). The *XMM-Newton* data do not allow such an effect to be resolved in AX J1813–178. A search for a steepening in the data with respect to the distance of the best fit centroid yielded no conclusive results within statistical errors. Nevertheless, it seems very likely that AX J1813–178 is indeed a PWN, as the positional coincidence of a hard spectrum X-ray source within a radio shell of G12.82–0.02 is otherwise very unlikely. Furthermore, a chance positional coincidence of the VHE γ-ray source HESS J1813−178 with this composite radio/X-ray object also seems unlikely, and in the following discussion we will assume that the emission seen in these three wavebands originates in a single new composite SNR, similar in its properties to e.g. G 0.9+0.1 (Aharonian et al. 2005c). However, the situation in the case discussed here is somewhat different, since the VHE γ-ray source shows extended emission (possibly owing to the smaller distance of HESS J1813−178 (∼4 kpc) in comparison to G 0.9+0.1 (∼8 kpc)).

Both the shell of the SNR as well as the newly found PWN candidate AX J1813–178 are viable γ-ray emitting objects. To estimate whether the shell of the SNR could be responsible for

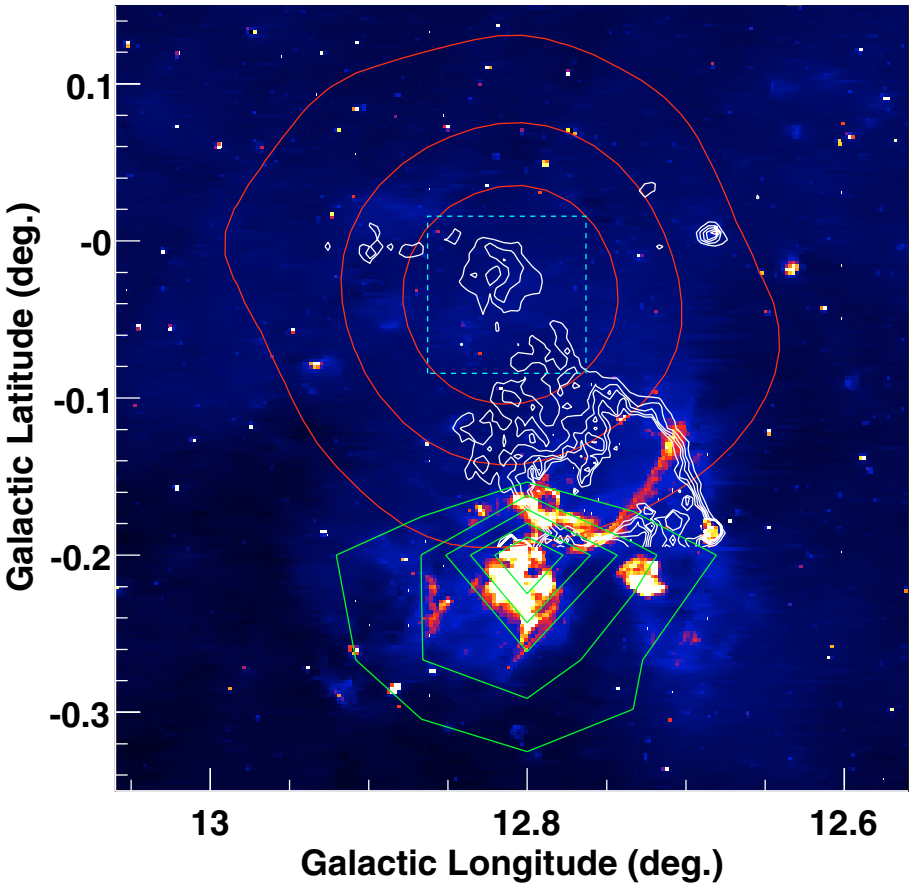

Fig. 5. *Spitzer* Space telescope data of the GLIMPSE survey at 8 μm (Benjamin et al. 2003) shown in Galactic coordinates. The red contours show again the HESS VHE γ-ray excess emission (smoothed with a Gaussian of 0.05° width and plotted in equidistant excess contours), whereas the white contours show the 20 cm VLA contours (Brogan et al. 2005). The green contours show the NANTEN CO-Emission contours at the distance of 4 kpc, showing the position of the GMC. The dashed cyan box indicates the size of the area shown in Fig. 2. No dust emission is coincident with the VHE γ-ray source as reported already by Brogan et al. (2005), supporting the non-thermal nature of the source. The *Spitzer* and NANTEN data are clearly correlated on this scale.

the γ-ray emission the following prescription has been followed: a background (determined in a ring of 2−4′ around the SNR centre) has been subtracted from the central 2′ radio emission, the resulting radio map has been smoothed with a Gaussian kernel of width $r_{\rm smooth} = 1.2'$, slices have been fit through the resulting smoothed map in RA- and Dec-Direction with Gaussians to determine σ_x and σ_y of the smoothed emission region. Finally the "Gaussian equivalent width" of the SNR has been defined as $\sigma_{\rm SNR} = (\sigma_x^2 + \sigma_y^2 - r_{\rm smooth}^2)^{1/2}$, yielding $\sigma_{\rm SNR} \approx 1.8'$, compatible with the measured rms extension $2.16' \pm 0.36'$ of the VHE γ-ray emission region. The SNR shell seems therefore to be a plausible candidate for the origin of the γ-ray emission.

As a result, we have to conclude that even with high angular resolution *XMM-Newton* X-ray observations in which the central X-ray emitting object AX J1813−178 was resolved, no final distinction can be drawn between the scenario in which the γ-rays originate in the shell or in the core of G12.82–0.02. The X-ray data described here and previously described radio observations indicate that G 12.82–0.02 is a composite supernova remnant with a bright X-ray core and a radio shell. The size of the gamma-ray source measured by HESS appears to be consistent with an origin of high energy emission in the SNR shell, but a common origin of the X-ray and γ-ray emission in a central PWN cannot be excluded as a larger spatial extent of the γ-ray source with respect to the X-ray source could occur in such cases (see for example the case of HESS J1825−137, Aharonian et al. 2006c), due to the energy dependent cooling of electrons. Two distinct scenarios for the origin of the TeV emission must therefore me considered: 1) as a counterpart to the X-ray emitting core, and 2) as a counterpart to the radio emission of the shell.

Scenario 1) has previously been discussed by Ubertini et al. (2005) and Helfand et al. (2005). Here the situation is revisited in the light of the new *XMM-Newton* data. Figure 6 (top) shows the spectral energy distribution of G 12.82–0.02. The EGRET upper limit has been derived from the first 5 years of the EGRET mission yielding a flux upper limit of 2.7×10^{-11} erg cm^{-2} s^{-1} above 100 MeV. Where angular resolution is sufficient (i.e. in the radio and <15 keV X-ray bands) the core and shell of the remnant are shown separately. Two synchrotron/Inverse Compton model curves are shown for a population of relativistic electrons in the core. The model was chosen to be time-dependent with constant injection over the lifetime of the source. The key model parameters are the slope of the injection spectrum of electrons α the minimum and maximum energies of the electrons $E_{\rm min}$ and $E_{\rm max}$, the magnetic field in the source B, and the target radiation field (CMBR, optical or dust photons). In both cases shown, an age of 1000 years is adopted, in-line with the estimates of Brogan et al. (2005) for the age of the remnant: 300−3000 years. The combined *XMM-Newton*/INTEGRAL spectrum indicates that $E_{\rm max}$ must be rather high: $\sim 10^{15}$ eV. If inverse Compton emission takes place in the Thompson regime then equal keV synchrotron X-ray and VHE γ-ray IC spectral indices are expected away from any cut-off in the electron spectrum. The softer spectrum measured by HESS therefore suggests that Klein-Nishina (KN) effects may be important in this source. The well-detected X-ray peak determines roughly a convolution of the magnetic field with the square of the maximum electron energy $B \times E_{\rm max^2}$, whereas the ratio of the total synchrotron to IC emission determines the ratio of B^2 to the radiation density. Therefore the electron index α is the only free parameter in the modelling when assuming typical radiation fields. A rather soft electron spectrum is needed to match the γ-ray data, whereas the X-ray data suggests a harder spectrum. The dashed lines in Fig. 6 (top) show a model with $\alpha = 2.4$, $B = 4.2$ μG, $E_{\rm min} = 25$ GeV, $E_{\rm max} = 1.5$ PeV and

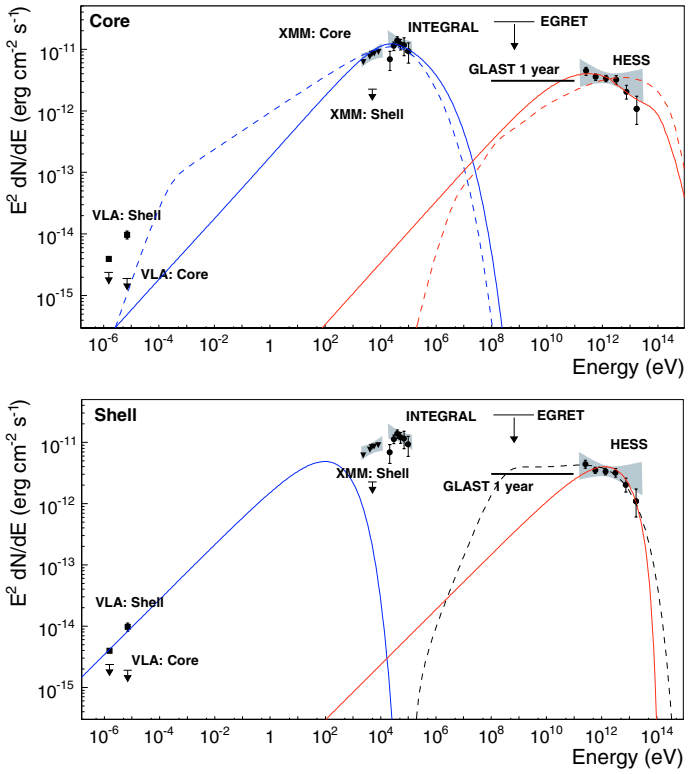

Fig. 6. Spectral energy distribution for HESS J1813−178. The *XMM-Newton* data 2 keV and 10 keV are shown for an extraction radius of 75′′ and are corrected for the absorption. A systematic error band of 0.2 on the spectral index and 20% on the flux level has been added. For the INTEGRAL points the data published in Ubertini et al. (2005) have been recently reanalysed to determine error bars on the flux points. The flux points shown here are consistent with the published points. The HESS spectrum has been rebinned in comparison to the energy spectrum shown in Aharonian et al. (2006a). Also shown is the 1-year integral sensitivity of the GLAST-LAT above 100 MeV taking into account both the instrumental background and the diffuse γ-ray emission in the Galactic plane. *Top*: scenario in which the VHE γ-ray emission originates in the core of the SNR (i.e. the PWN). Leptonic one-zone model (Aharonian & Atoyan 1999) for two scenarios in which the VHE γ-ray emitting and the X-ray emitting electrons belong to the same population. The model parameters are specified in the text. *Bottom*: scenario in which the VHE γ-ray emission originates in the radio shell of the SNR. Leptonic (solid) and hadronic (dashed) VHE γ-ray emission scenarios in which the γ-ray emission originates in the shell of the SNR, i.e. the radio and VHE γ-ray emitting electrons are connected.

a radiation field with near and far infra-red components each of energy density 1 eV cm^{-3} in addition to the CMBR. Such a scenario is in marginal agreement with the HESS and X-ray data, but a low energy break or cut-off in the electron spectrum is required to avoid over-producing radio emission in the SNR core. This cutoff could be explained by the termination shock of a PWN, in which the electrons in the lab-system have gained a minimum energy through bulk motion. This minimum energy can be as high as ∼100 GeV up to 1 TeV, for a typical PWN Lorentz factor between 10^5 and 10^6. The spectral break can be avoided by invoking a strong contribution of scattering by IR/optical radiation fields, where IC scattering transits into the KN regime and is thus cut off at higher energies, resulting in an apparent steepening of the VHE γ-ray spectra compared to the X-ray spectra. The solid curves in Fig. 6 (top) show a model with $\alpha = 2$, $B = 7.5\ \mu$G, $E_{\rm min} = 1$ MeV, $E_{\rm max} = 1.5$ PeV and a radiation field with a very strong NIR component, with energy density 1000 eV cm^{-3}. This radiation field exceeds by a factor of ≈1000 the nominal NIR radiation field at 4 kpc from the Galactic Centre (see e.g. Porter et al. 2006) and is thus somewhat unrealistic. The (possibly) nearby star forming region W 33 may contribute to the radiation density in the vicinity of the source. However, Helfand et al. (2005) have estimated the radiation density in G 12.82–0.02 to be 3−4 eV cm^{-3}, including the contribution of W 33. Scenarios with intermediate values provide equally acceptable agreement with the available data. See Hinton & Aharonian (2007) for details of the calculation methods used here.

A leptonic model, in which the core X-ray and VHE γ-ray emission are associated, yields an unavoidable $E_{\rm max} > 1$ PeV, suggesting that HESS J1813–178 is a highly effective accelerator – a Galactic *Pevatron*. In case of a soft electron injection spectrum $E_{\rm max}$ could well be higher, since the *XMM-Newton*–INTEGRAL spectral break could plausibly be a cooling break, rather than represent the end of the electron spectrum, for a somewhat greater pulsar age. If the X-ray and VHE γ-ray emission are indeed associated (i.e. originate from the same electron population), the PeV maximum energy for the accelerated electrons implies the emission almost certainly has plerionic origin. PWN are certainly capable of accelerating electrons to PeV energies as e.g. shown by EGRET measurements of the Crab Nebula, showing a synchrotron component extending to MeV energies (shell type SNRs in the framework of diffusive shock acceleration scheme fall short of 1 PeV for *electron* acceleration). The total energy injected in the electrons is 6×10^{46} erg for the high-IR case and even 6×10^{47} erg for the soft electron spectrum case. For a source of age 1000 years (as suggested by Brogan et al. 2005) these values result in an electron luminosity of $L_{\rm e} \sim 2 \times 10^{36}$–$2 \times 10^{37}$ erg/s. This value can be compared to that of the PWN in the composite SNR G 0.9+0.1 which has a inferred electron luminosity of $L_{\rm e} \sim 7 \times 10^{37}$ erg/s (Hinton & Aharonian 2007).

A distinct alternative scenario is an origin of the γ-ray emission in the SNR shell. Two young shell-type SNRs (with estimated ages comparable to that of G 12.82–0.02) are well established VHE γ-ray sources, namely RX J1713.7–3946 and RX J0852.0–4622 (known as *Vela Junior*). Placed at the greater distance of 4 kpc, the TeV luminosity of HESS J1813–178 is comparable to that of these two SNRs. Furthermore, the measured size of the TeV emitting region is consistent with an origin in the radio shell. The SNR shell must therefore by considered seriously as an alternative source of the TeV emission. Figure 6 (bottom) shows two models for a γ-ray origin in the SNR shell: a) as inverse Compton emission from the electron population responsible for the radio emission (solid line), and b) as the product of the decay of neutral pions produced in hadronic interactions of accelerated protons in or near the SNR shell (dashed line), calculated using the parametrisation of Kelner et al. (2006). In either case, the central X-ray emission must be attributed to a different mechanism, presumably a PWN. The electron model has parameters: $\alpha = 2.1$, $B = 5\ \mu$G, $E_{\rm min} = 1$ MeV, $E_{\rm max} = 30$ TeV and a nominal 4 kpc radiation field (note that larger values of $E_{\rm min}$ up to 1 GeV are still compatible with the radio emission). The small value of $E_{\rm max} = 30$ TeV is required to avoid producing significant X-ray synchrotron emission in the shell. For values much larger than this, 2 keV emission from the shell should have been seen in this *XMM-Newton* observation. The proton model has $\alpha = 2.1$, $E_{\rm min} = 1$ GeV, $E_{\rm max} = 100$ TeV. To match the TeV flux level in the p-p interaction scenario the product of the total energy in protons and the ambient density must be: $(E_{\rm p}/10^{50}\,{\rm erg})(n/1\ {\rm cm}^{-3}) \approx 1$. For

likely densities greater than 1 cm^{-3}, the required acceleration efficiency is <10% for a typical SNR explosion energy of 10^{51} erg. In case of a very large local density, Bremsstrahlung effects start to become important and might increase the VHE γ-ray flux in comparison to the synchrotron X-ray flux. However, as we consider most of the absorption in the X-ray spectrum to be foreground density, the density within the source is likely insufficient for Bremsstrahlung to be the dominant process.

5. Summary and Conclusion

Detailed *XMM-Newton* X-ray and NANTEN ^{12}CO(J = 1−0) studies have been performed towards the γ-ray source HESS J1813−178. The NANTEN data show a giant molecular cloud in the vicinity of HESS J1813−178 that might have played an important role in the evolution of the γ-ray source. The X-ray data show a resolved non-thermal object in the centre of the shell of the radio SNR, most likely representing synchrotron emission from a PWN. The confirmation of this picture would require the detection of a central pulsar, either in X-ray or in radio observations, or indirectly through the detection of spectral cooling as seen in several other PWN systems. Nevertheless, G 12.82–0.02 is now tentatively established as a *composite SNR* through its distinct morphology of a central extended non-thermal object within a radio shell. For the first time, an object of this type has been detected first in VHE γ-rays and then identified with high-angular resolution radio and X-ray data. This detection shows, that γ-ray observations are well suited to identify SNR, that are otherwise very hard to detect due to obscuration. No distinction is so far possible between a scenario in which the γ-rays are emitted from the shell of the SNR, and one in which they are emitted from the central PWN. An upcoming deep Suzaku exposure on HESS J1813−178 will shed more light on the situation in the hard X-ray band and the future GLAST satellite will provide important constraints in the MeV−GeV band. If the central X-ray source and the VHE γ-ray source are indeed connected our modelling of the SED emission suggests that HESS J1813−178 is a Galactic Pevatron.

Acknowledgements. The authors would like to acknowledge the support of their host institutions, and additionally support from the German Ministry for Education and Research (BMBF). Specifically, SF acknowledges support of the Department of energy (DOE). JAH is supported by a UK Particle Physics & Astronomy Research Council (PPARC) Advanced Fellowship. We would like to thank the whole HESS collaboration for their support. We would also like to thank Y. Uchiyama for providing the analysis of the ASCA data. SF would like to thank C. Brogan and B. Gaensler for useful discussions on this source.

References

Aharonian, F. A. 1991, Ap&SS, 180, 305
Aharonian, F. A., & Atoyan, A. 1999, A&A, 351, 330
Aharonian, F. A., et al. (HESS Collaboration) 2005a, Science, 307, 1938
Aharonian, F. A., et al. (HESS Collaboration) 2005b, Science, 309, 746
Aharonian, F. A., et al. (HESS Collaboration) 2005c, A&A, 432, 25
Aharonian, F. A., et al. (HESS Collaboration) 2006a, ApJ, 636, 777
Aharonian, F. A., et al. (HESS Collaboration), 2006b, A&A, 460, 743
Aharonian, F. A., et al. (HESS Collaboration) 2006c, A&A, 460, 365
Albert, J. 2006, ApJ, 673, L41
Benjamin, R. A., Churchwell, E., Babler, Brian, L., et al. 2003, PASP, 115, 953
Bertsch, D. L., Dame, T. M., Fichtel, C. E., et al. 1993, ApJ 416, 587
Brand, J., & Blitz, L. 1993, A&A, 275, 67
Brogan, C. L., Gaensler, B. M., Gelfand, J. D., et al. 2005, ApJ, 629, L105
Churchwell, E. 1990, A&ARv, 2, 79
Dickey, J. M., & Lockman, F. J. 1990, ARA&A, 28, 215
Funk, S. 2007, Ap&SS, 309(1-4) [arXiv:astro-ph/0609586]
Goldsmith, P. F., & Mao, X.-J. 1983, ApJ, 265, 791
Gaensler, B. M., & Slane, P. O. 2006, ARA&A, 44, 17
Helfand, D. J., Becker, R. H., & White, R. L. 2005, ApJL, submitted [arXiv:astro-ph/0505392]
Hinton, J. A., & Aharonian, F. A. 2007, ApJ, 657, 302
Kelner, S. R., Aharonian, F. A., & Bugayov, V. V. 2006, Phys. Rev. D, 74, 034018
Landi, R., Bassani, L., Malizia, A., et al. 2006, ApJ, 651, 190
Manchester, R. N. 2001, MNRAS, 328, 17
Mitchell, G. F., Maillard, J.-P., Allen, M., et al. 1990, ApJ, 363, 554
Mizuno, A., & Fukui, Y. 2004, ASP Conf. Ser., 317, 59
Porter, T. A., Moskalenko, I. V., & Strong, A. W. 2006, ApJ, 648, L29
Reach, W. T., Rho, J., Tappe, A., et al. 2006, AJ, 131, 1479
Reifenstein, E. C., Wilson, T. L., Burke, B. F., et al. 1970, A&A, 4, 357
Slane, P., Yang, C., Schulz, N. S., et al. 2000, ApJ, 533, L29
Snowden, S. L, Collier, M. R., & Kuntz, K. D. 2004, ApJ, 610, 1182
Sugizaki, M., Mitsuda, K., Kaneda, H., et al. 2001, ApJS, 134, 77
Ubertini, P., Bassani, L., Malizia, A., et al. 2005, ApJ, 629, L109
White, R. L., Becker, R. H., & Helfand, D. J. 2005, AJ 130, 586

A&A 469, L17–L21 (2007)
DOI: 10.1051/0004-6361:20066836

Astronomy & Astrophysics

Letter to the Editor

XMM-Newton observations of the first unidentified TeV gamma-ray source TeV J2032+4130⋆

D. Horns[1], A. I. D. Hoffmann[1], A. Santangelo[1], F. A. Aharonian[2], and G. P. Rowell[3]

[1] Institute for Astronomy and Astrophysics Tübingen (IAAT) Sand 1, 72076 Tübingen, Germany
e-mail: horns@astro.uni-tuebingen.de
[2] Max-Planck Institut für Kernphysik (MPIK) PO Box 10 39 80, 69117 Heidelberg, Germany
[3] School of Chemistry and Physics, University of Adelaide, Australia

Received 29 November 2006 / Accepted 26 April 2007

ABSTRACT

Context. The first unidentified very high energy gamma ray source (TeV J2032+4130) in the Cygnus region has been the subject of intensive search for a counterpart source at other wavelengths. In particular, observations in radio and X-rays are important to trace a population of non-thermal electrons.
Aims. A deep (≈50 ks) exposure of TeV J2032+4130 with *XMM-Newton* has been obtained. The large collection area and the field of view of the X-ray telescopes on-board of *XMM-Newton* allow to search for faint extended X-ray emission possibly linked to TeV J2032+4130.
Methods. The contribution of point sources to the observed X-ray emission from TeV J2032+4130 is subtracted from the data. The point-source subtracted X-ray data are analyzed using blank sky exposures and regions adjacent to the position of TeV J2032+4130 in the field of view covered by the XMM-Newton telescopes to search for diffuse X-ray emission.
Results. An extended X-ray emission region with a full width half maximum (*FWHM*) size of ≈12 arcmin is found. The centroid of the emission is co-located with the position of TeV J2032+4130. The angular extension of the X-ray emission region is slightly smaller than the angular size of TeV J2032+4130 (*FWHM* =14 ± 3 arcmin). The energy spectrum of the emission coinciding with the position and extension of TeV J2032+4130 can be modeled by a power-law model with a photon index $\Gamma = 1.5 \pm 0.2_{\rm stat} \pm 0.3_{\rm sys}$ and an energy flux integrated between 2 and 10 keV of $f_{2-10\,\rm keV} \approx 7 \times 10^{-13}$ erg/(cm^2 s) which is lower than the very high energy gamma-ray flux observed from TeV J2032+4130. The energy flux detected from the extended emission region is about a factor of two smaller than the summed contribution of the point sources present. The energy spectrum can also be fit with a thermal emission model from an ionized plasma with a temperature $k_{\rm B}T \approx 10$ keV.
Conclusions. We conclude that the faint extended X-ray emission discovered in this observation is the X-ray counterpart of TeV J2032+4130. Formally, it can not be excluded that the extended emission is due to an unrelated population of faint, hot ($k_{\rm B}T \approx 10$ keV) unresolved point-sources which by chance coincides with the position and extension of TeV J2032+4130. We discuss our findings in the frame of both hadronic and leptonic gamma-ray production scenarios.

Key words. acceleration of particles – gamma rays: observations – X-rays: general – gamma rays: theory

1. Introduction

Ground based air Cherenkov telescopes have detected in the last 6 years a number of unidentified sources of very high energy (VHE, $E > 100$ GeV) gamma-rays located in the Galactic plane. The first representative of these sources (TeV J2032+4130) was discovered serendipitously with the HEGRA telescope system in the Cygnus region (Rowell & Horns 2002; Aharonian et al. 2002).

In a subsequent deep exposure for a total of ≈280 h of observation time the source detection was confirmed and its properties were studied in detail (Horns & Rowell 2004; Aharonian et al. 2005a).

A remarkable feature of TeV J2032+4130 is the fact that the angular extension of the source is $(6.2 \pm 1.2_{\rm stat} \pm 0.9_{\rm sys})$ arcmin in radius which corresponds to a *FWHM* = 14 arcmin. Gamma-ray emission from TeV J2032+4130 has been confirmed independently by the Whipple collaboration (Lang et al. 2004; Konopelko et al. 2006). A gamma-ray excess from the Cygnus region albeit more extended was recently reported by the Milagro collaboration (Abdo et al. 2006). The properties of TeV J2032+4130 are common to most of the other unidentified VHE gamma-ray sources that have been discovered with the HESS telescopes so far (Aharonian et al. 2005b, 2006a): TeV J2032+4130 can be considered as the proto-type of the unidentified VHE gamma-ray sources known today.

So far, a number of point-like or moderately extended candidates for counterparts of TeV J2032+4130 have been identified at radio (Paredes et al. 2006; Butt et al. 2006b) and X-rays (Butt et al. 2003, 2006a; Mukherjee et al. 2003, 2006).

The origin and nature of TeV J2032+4130 remains unclear. It has been suggested that the nearby ($d = 1.7$ kpc) massive stellar OB association Cyg OB2 (see e.g. Knödlseder 2000) could be an accelerator of charged cosmic rays and consequently a site of gamma-ray production (Aharonian et al. 2002; Butt et al. 2006a; Aharonian et al. 2006b). This scenario has been strengthened by the recently discovered spatially extended

⋆ Based on observations obtained with XMM-Newton, an ESA science mission with instruments and contributions directly funded by ESA Member States and NASA.

VHE gamma-ray emission from the direction of the open stellar cluster Westerlund 2 (Aharonian et al. 2007).

Other possible explanations for the nature of TeV J2032+4130 have been brought forward including gamma-ray production in possible jet lobes of Cyg X-3 (Aharonian et al. 2002), an unknown pulsar wind nebula (Bednarek 2003), or even extra-galactic source candidates as suggested by Mukherjee et al. (2003) and Butt et al. (2006b).

Independent of the nature of the source, two different gamma-ray production mechanisms are generally considered. In the *hadronic scenario*, gamma-rays are produced mainly via inelastic scattering of accelerated nuclei with the ambient medium (see e.g. Aharonian et al. 2005a; Reimer et al. 2006; Domingo-Santamaría & Torres 2006). Alternatively, in the *leptonic* scenario gamma-rays are produced via inverse Compton scattering of ambient photons from a population of energetic electrons (Aharonian et al. 2005a; Reimer et al. 2006). Recently, it has been suggested, that excitation of giant dipole resonances of relativistic heavy nuclei in radiation dominated environments could be responsible for gamma-ray production in Cyg OB2 (Anchordoqui et al. 2006).

While the gamma-ray observations so far have been inconclusive with respect to the origin of the observed signal, X-ray observations can provide additional information to identify the origin of the emission and to discern between the two proposed scenarios.

In this *Letter*, we report the detection of spatially extended X-ray emission coinciding with the position of TeV J2032+4130.

2. Observations and data analyses

The data were taken during two separate pointings of *XMM-Newton*. Table 1 summarizes the available data and configurations of the instruments used. The data were screened for soft proton flares following the method suggested in Read & Ponman (2003). The detectors performed almost nominally: CCD #6 of the MOS 1 camera had been switched off and CCD #5 of MOS2 shows an increased instrumental background below 1 keV which is two times larger than the background seen in the adjacent CCDs #4 and #6. However, above 1 keV the background rate in CCD #5 appeared consistent with the other detectors. The data suffer from contamination of single scattering events from the bright X-ray source Cyg X-3. The contamination is most prominent in the energy band above 5 keV. For this reason, the analyses that have been performed are constrained on the energy range from 1–5 keV where the instrumental background and stray light contamination from Cyg X-3 are minimal. A closer inspection of the contamination using ray-tracing simulations has shown that the contribution of scattered light from Cyg X-3 to the X-ray emission seen from TeV J2032+4130 is negligible. At the same time, the vignetting of the telescopes is smallest in this energy range (Kirsch 2006; Pradas & Kerp 2005).

Data reduction and analyses were performed using the Standard XMM-Newton Science Analysis Software *SAS* v7.0.

2.1. Search for diffuse X-ray emission

In an initial step of the data analyses, a catalogue of sources detected in the 1–5 keV energy range is assembled using the `edetect_chain` task simultaneously for the MOS1, MOS2, and EPIC pn cameras for each of the two exposures. The minimum detection likelihood is set to a low value of 2. This way, 13.5% of the detected sources are due to statistical fluctuations while at the same time, more and fainter sources are detected than with the default value of 10. A detailed study of the point sources detected in this XMM-Newton observation will be presented elsewhere. Here, the source catalogue has been used to generate model images of the point sources separately for each camera and pointing taking into account the position dependent point spread function of the XMM-Newton mirrors. These model images are then subtracted off the individual frames of the three cameras and for the two pointings. Within the 6.2′ region covered by the extension of the TeV source, a total energy flux of $f_{1-5\ \mathrm{keV}} \approx 10^{-12}$ erg/(cm^2 s) associated with point sources is observed. In order to subtract the particle and extragalactic photon background blank sky event files for the corresponding observation modes and filter settings have been obtained from the XMM guest observers' facility[1]. The blank field data have been processed to match the observational data and the resulting images are subtracted off the pointings towards TeV J2032+4130. The images for the MOS1 and MOS2 cameras obtained from the two exposures are combined to form a background subtracted mosaic. The images of the EPIC pn camera have been omitted because of artefacts resulting from oversubtracting the contribution of point sources. For each of the four remaining images, exposure maps have been generated using the SAS task eexpmap. The exposure maps are combined in a mosaic which is then trimmed to a minimum exposure of 5 ks corresponding to roughly 5% of the peak value. The background subtracted mosaic is then divided by the exposure map to obtain an exposure corrected, background subtracted, and source free image. Figure 1 shows three images of the combined exposures of the MOS1 and MOS2 cameras before the subtraction of the model images of the point sources (a), after the subtraction and smoothing with Gaussian of fixed width of 45 arcsec (b), and finally, the image after convolving it with a Gaussian of fixed width of 1.5 arcmin (c). Note the presence of scattered light along ring segments in the southern part of Fig. 1a. While Fig. 1b shows indications for the presence of a rim-like feature resembling the morphology observed in radio by Paredes et al. (2006), it should be noted that the subtraction of point-sources has an impact on the observed morphology on angular scales small compared to the extension of the detected extended emission. For a comparison with the extension and morphology of the gamma-ray source TeV J2032+4130, contours are overlaid to Fig. 1c. The X-ray image shows an extended emission region which is co-located with TeV J2032+4130 and of similar extension. The exposure corrected image of the diffuse emission is fit by a Gaussian with a width of (5.1 ± 0.3) arcmin which corresponds to a $FWHM$ = (11.7 ± 0.6) arcmin[2].

2.2. Energy spectrum of the diffuse X-ray emission

In order to determine the energy spectrum of the diffuse X-ray emission, the contribution of the point sources has to be removed by excising regions around the sources. We use an excising region adapted to the point spread function and brightness of the source. The size of the region is chosen such that the relative contribution of the source to the local background is less than 20% at the boundary of the excised region. The wings of the point spread function lead to a contamination of the detected diffuse emission which amounts to 27% of the excess

[1] `ftp://xmm.esac.esa.int`

[2] All errors given throughout the paper are to the confidence of one standard deviation.

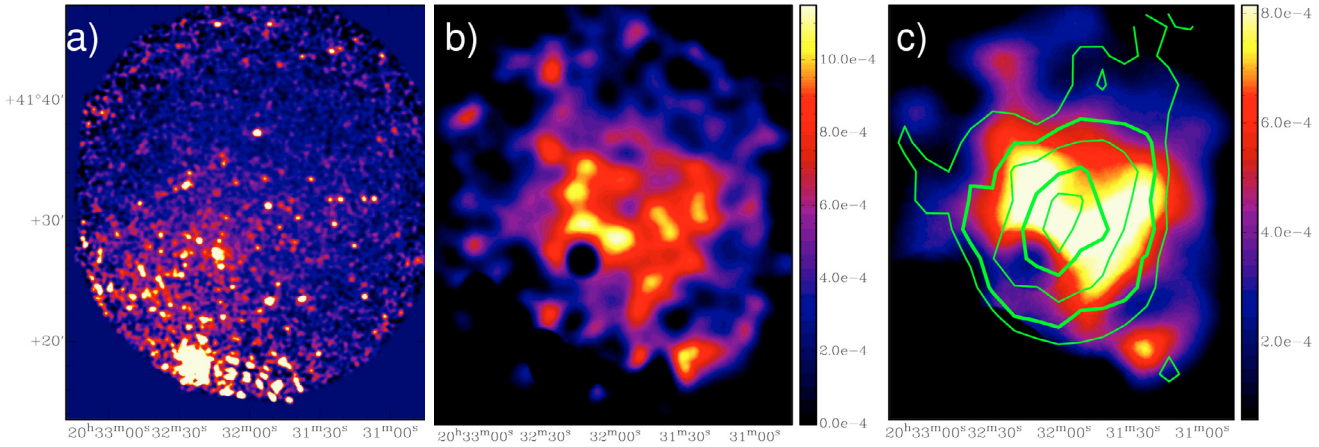

Fig. 1. Background subtracted and exposure corrected images obtained from the combined exposures of the MOS1 and MOS2 cameras (in units of counts/(s arcmin^2). While the left image shows the emission including all point sources, the middle image shows the image after subtracting off all point sources, smoothed with a Gaussion of 45 arcsec width and with a changed scaling to highlight the extended X-ray emission present. Finally, the right image is obtained by smoothing the source subtracted image with a Gaussian of 1.5 arcmin width. The green contours indicate (in linear spacing) the significance contour of the HEGRA observations (starting at 3σ).

signal seen. This effect of contamination would be however compensated by the opposite effect caused by the diffuse emission present in the excised region (≈25%) and therefore excluded from the reconstructed energy spectrum. We estimate the systematic uncertainty of this contamination to be 10% of the total flux. The energy spectra of a source region with a radius of 6.2′ centered on the position of TeV J2032+4130 from the MOS2 and EPIC pn cameras of the second pointing (ObsID 0305560201) are extracted. The second pointing is centered 5′ north of the centroid of TeV J2032+4130 and therefore, we can choose a background region which is mirrored through the center of the field of view and has a similar acceptance as the source extraction region. Using the background region in the same field of view, the background estimate includes all relevant background components including X-ray emission from the Galactic ridge and the particle and instrumental background specific to this observation. The small azimuthal modulation of the acceptance of the MOS cameras can be neglected along this direction. The MOS1 camera is not used because the disabled CCD#6 unfortunately does not allow to cover the entire source.

The response files are generated for these particular observations using the standard tools `arfgen` and `rmfgen`. Finally, the geometrical areas of the source and background regions are calculated taking gaps between the CCDs, bad pixels, and point source exclusion regions into account. The resulting background subtracted X-ray spectrum is fit with a power-law as well as an optically thin hot plasma model (`apec`) including photoelectric absorption (`phabs`). The spectral fitting of the two spectra was done using the `xspec` v11.3.2p spectral fitting package (Arnaud 1996). The fit describes the data well (see Table 2 for a summary of the fit parameters; only statistical 1σ errors are quoted).

In order to estimate the influence of faint, unresolved point sources present in the stellar cluster, we have reduced X-ray imaging data taken with the Chandra satellite (Obs.# 4501 for 48.6 ks on TeV J2032+4130 and Obs.# 4511 for 98.7 ks in the south-west of TeV J2032+4130, centered on the core of Cyg OB2). Based upon a comparison of the Chandra and XMM-Newton source catalogues and the study of the X-ray source population present in the Cyg OB2 cluster (Colombo et al. 2006), we estimate that point sources below the XMM-Newton detection limit can contribute up to ≈30% of the observed diffuse emission. It is however not straight-forward to correct the observed excess for the unresolved point sources detected with Chandra as the flux of the sources is generally found to vary with time. We estimate the systematic uncertainty on the flux conservatively to be 50% combining the influence of the unresolved point sources (≈30%), uncertainties on the background subtraction (≈10%), as well as the tails of the point spread functions of excised point sources (≈10%). The total, unabsorbed energy flux derived from the model fit (see Table 2) is found to be $f_{2-10} = (7.3 \pm 3.5_{\rm sys} \pm 1.1_{\rm stat}) \times 10^{-13}$ erg/(cm^2 s).

Table 1. Summary of observation times and configurations on the target "TeV J2032+4130". All instruments were operated in full frame mode with a medium filter. The exposure quoted in parenthesis is for the EPIC pn camera.

ObsID	Date	RA J2000	Dec J2000	Exposure [ks]
0305560101	2005-10-21	20:31:57	41:29:58	27.3(23.6)
0305560201	2005-10-25	20:31:57	41:34:55	25.8(20.5)

Table 2. Summary of the fit results of the X-ray energy spectrum with a power-law model (`powerlaw`) or thermal emission (`apec` with fixed solar abundances of the plasma) including photo-electric absorption (`phabs`).

Parameter	Value (powerlaw)	Value (apec)
$N_{\rm H}$ [10^{21} cm^{-2}]	3.5 ± 1.6	3.2 ± 1.1
Γ, $k_{\rm B}T$ [keV]	1.5 ± 0.2	10.5 ± 3.2
$f_{2-10\ \rm keV}$ [10^{-13} erg/(cm^2 s)]	7.3 ± 1.1	7.4 ± 1.1
$\chi^2_{\rm red}$ (d.o.f.)	1.02 (862)	1.01 (861)

3. Conclusions

The XMM-Newton observations presented here indicate the presence of an extended (*FWHM* = 11.7 arcmin) X-ray source co-located with the first unidentified VHE gamma-ray source TeV J2032+4130 discovered with the HEGRA air Cherenkov telescope system. The size of the X-ray source is similar to the one of TeV J2032+4130. The energy spectrum

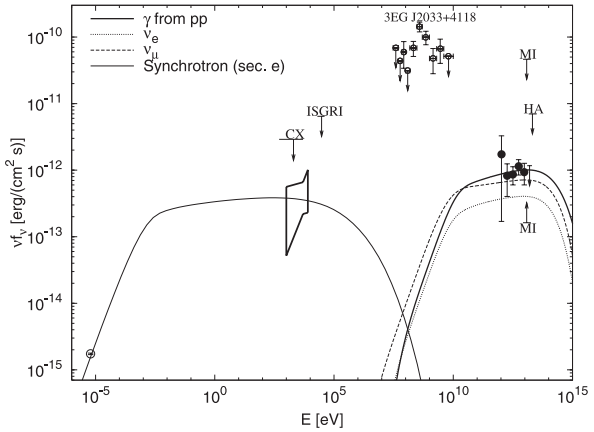

Fig. 2. The spectral energy distribution of TeV J2032+4130: the bow-tie indicates the energy spectrum as measured with XMM-Newton including systematic and statistical uncertainties. The lines indicate the result of a model calculation for a hadronic gamma-ray and neutrino production scenario for a continuously active accelerator of protons up to a maximum energy of 5 PeV at an age of $t_{\rm age} = 2500$ yrs and magnetic field $B = 1$ mG. The radio flux point of a possible non-thermal extended radio-source at $\lambda = 20$ cm (Paredes et al. 2006) is assumed to be an upper limit to the actual radio emission associated with TeV J2032+4130. The upper limits between 0.5–5 keV (CX, Chandra) and 20–40 keV (ISGRI, INTEGRAL) are taken from Butt et al. (2006a). The energy spectrum of the EGRET source 3EG J2030+4118 (Hartman et al. 1999) is considered to be an upper limit. The Milagro (MI) upper limit is the integrated emission in a 3×3 $(^\circ)^2$ region (Abdo et al. 2006) while the lower limit (MI) is scaled to the solid angle covered by TeV J2032+4130 assuming a uniform surface brightness. The upper limit from the HEGRA-AIROBICC (HA) wide angle Cherenkov detector is taken from Aharonian et al. (2002).

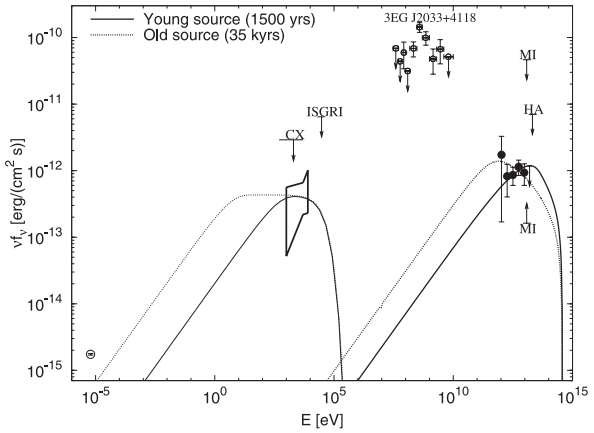

Fig. 3. In the leptonic scenario, the data are described well by a young source of an age of 1500 yrs, a magnetic field of $B = 3\,\mu$G and an energy density of the seed photon field of $w_{\rm IR} = 3$ eV/cm^3 with a grey body temperature of $T = 10$ K. As an alternative, an older source at an age of 35 kyrs is shown ($B = 3\,\mu$G, $w_{\rm IR} = 1$ eV/cm^3). For a description of the multi-wavelength data see the caption of Fig. 2.

can be fit by a power-law model or by a thermal emission model with a plasma temperature of $k_{\rm B}T \approx 10$ keV. The unabsorbed energy flux of the X-ray source in the energy range from 2–10 keV is a factor of 2–3 smaller than the one observed from TeV J2032+4130 at energies from 1–10 TeV.

We note that the observed extended X-ray emission could in principle be a so far unknown population of faint X-ray sources that are by chance distributed at an angular size which is similar to the one of TeV J2032+4130. The energy spectrum of these sources would have to be different from the bulk of the stellar X-ray sources detected from Cyg OB2 (Colombo et al. 2006) which on average show a thermal spectrum with $k_{\rm B}T \approx 1 \ldots 3$ keV. Taking these considerations into account, we conclude that the observed extended X-ray emission is the X-ray counterpart of TeV J2032+4130.

Initial modeling of the X-ray and gamma-ray energy spectra using a hadronic gamma-ray production scenario indicates that the observed spectra can be naturally explained by a young (a few kyrs) "Pevatron" accelerator. The observation of synchrotron X-ray emission up to ≈5 keV constrains the product of the square of maximum energy of accelerated protons $E^2_{\rm max}$) and magnetic field (B) to exceed $E^2_{\rm max} \cdot B \gtrsim 5$ PeV^2 mG. In this picture, the gamma-ray energy spectra would continue without cut-off well beyond 10 TeV. The hard X-ray emission from a similar source size region as the gamma-ray emission is a natural prediction within this model where the X-rays are produced by synchrotron emission of secondary electrons. Notably, in the frame of this model, the extended gamma-ray emission found by the Milagro collaboration would be explained by gamma-rays produced by accelerated particles of energies ≳100 TeV which have already escaped the accelerator.

A leptonic scenario provides a valid explanation of the observations as well (see Fig. 3). In this scenario, a young accelerator with a low magnetic field of a few μG accelerating electrons following a power-law distribution with $\mathrm{d}N/\mathrm{d}E \propto E^{-2}$ reaching up to energies of a few 100 TeV can provide a good fit to the X-ray and gamma-ray data. In contrary to the hadronic scenario, the gamma-ray energy spectrum above 10 TeV is expected to be rather soft due to un-avoidable Klein-Nishina suppression of inverse Compton scattering. Furthermore, the seed photon density has to be higher than the average value in the interstellar medium (which is not unlikely given the possible proximity to the Cyg OB2 stellar association and the large stellar extinction towards that region indicating high density of dust). In the leptonic scenario, the X-ray spectrum can be expected to vary at different parts of the source due to cooling effects. More X-ray observations will be required to detect spectral variability.

Finally, neutrino observations will prove decisive to discern between the two emission scenarios (since neutrinos are only expected in the hadronic scenario). Even though the neutrino flux calculated here is very likely not detectable with the coming generation of neutrino telescopes like IceCube (Achterberg et al. 2006), it may be that the gamma-ray flux detected with Milagro from the same region is tracing the high energy particles which have already left the accelerator and fill a much larger volume. In this case, the region *around* TeV J2032+4130 would be a powerful high energy neutrino source and would be detectable with future neutrino telescopes (Beacom & Kistler 2007).

It should be noted that the observations of TeV J2032+4130 carried out with XMM-Newton are so far the deepest observations available for any of the unidentified VHE gamma-ray sources. It will be interesting to perform similar observations to search for faint, extended X-ray counterparts of other unidentified VHE gamma-ray sources.

Acknowledgements. We acknowledge the support of the Deutsches Zentrum für Luft- und Raumfahrt under grant number 50OR0302 and the support of the Eberhard Karls Universität Tübingen. We wish to thank Olaf Reimer and Facundo Albacete for providing the source lists found in the Chandra observations and Josep Paredes for making their results available prior to publication. This research has made use of NASA's Astrophysics Data System. We thank the anonymous referee for valuable comments.

References

Abdo, A. A., Allen, B., Berley, D., et al. 2007, ApJ, 658, L33
Achterberg, A., et al. (Icecube Collaboration) 2006, Astropart. Phys., 26, 155
Aharonian, F., et al. (HEGRA coll.) 2002, A&A, 393, L37
Aharonian, F., et al. (HEGRA coll.) 2005a, A&A, 431, 197
Aharonian, F., et al. (HESS coll.) 2005b, Science, 307, 1938
Aharonian, F., et al. (HESS coll.) 2006a, ApJ, 636, 777
Aharonian, F., et al. (HEGRA coll.) 2006b, A&A, 454, 775
Aharonian, F., et al. (HESS coll.) 2007, [arXiv:astro-ph/0703427]
Albacete Colombo, J. F., Flaccomio, E., Micela, G., Damiani, F., & Sciortino, S. 2007, A&A, 464, 211
Anchordoqui, L. A., Beacom, J. F., Goldberg, H., Palomares-Ruiz, S., & Weiler, T. J. 2007, Phys. Rev. D, 75, 063001
Arnaud, K. A. 1996, Astronomical Data Analysis Software and Systems V, ASP Conf. Ser., 101, 17
Beacom, J. F., & Kistler, M. D. 2007, Phys. Rev. D, submitted, [arXiv:astro-ph/0701751]
Bednarek, W. 2003, MNRAS, 345, 847
Butt, Y. M., Benaglia, P., Combi, J. A., et al. 2003, ApJ, 597, 494
Butt, Y. M., Drake, J., Benaglia, P., et al. 2006a, ApJ, 643, 238
Butt, Y. M., Combi, J. A., Drake, J., et al. 2006b, ApJ, submitted, [arXiv:astro-ph/0611731]
Domingo-Santamaría, E., & Torres, D. F. 2006, A&A, 448, 613
Hartman, R. C., Bertsch, D. L., Bloom, S. D., et al. 1999, ApJS, 123, 79
Horns, D., & Rowell, G. 2004, New Astron. Rev., 48, 489
Horns, D., Aharonian, F., Santangelo, A., Hoffmann, A. I. D., & Masterson, C. 2006, A&A, 451, L51
Kelner, S. R., Aharonian, F. A., & Bugayov, V. V. 2006, Phys. Rev. D, 74, 034018
Kirsch, M. 2006, in internal report XMM-SOC-CAL-TN-0018
Konopelko, A., et al. 2006, ApJ, accepted, [arXiv:astro-ph/0611730
Knödlseder, J. 2000, A&A, 360, 539
Lang, M. J., Carter-Lewis, D. A., Fegan, D. J., et al. 2004, A&A, 423, 415
Mukherjee, R., Halpern, J. P., Gotthelf, E. V., Eracleous, M., & Mirabal, N. 2003, ApJ, 589, 487
Mukherjee, R., Gotthelf, E. V., & Halpern, J. P. 2006, [arXiv:astro-ph/0610299]
Paredes, J. M., Marti, J., Ishwara Chandra, C. H., & Bosch-Ramon, V. 2007, ApJ, 654, 135
Pradas, J., & Kerp, J. 2005, A&A, 443, 721
Read, A. M., & Ponman, T. J. 2003, A&A, 409, 395
Reimer, A., Pohl, M., & Reimer, O. 2006, ApJ, 644, 1118
Rowell, G., & Horns, D. 2002, In Proceedings of The Gamma-Ray Universe, ed. A. Goldwurm, Les Arcs, France, 385
Waldron, W. L., Corcoran, M. F., Drake, S. A., & Smale, A. P. 1998, ApJS, 118, 217